Diyala Journal of Engineering Sciences

Journal homepage: https://djes.info/index.php/djes

ISSN: 1999-8716 (Print); 2616-6909 (Online)

Beyond ISO Approximations: Tool-Path-Based Analytical Modelling of Root Fillets in Altered-Tooth-Sum Spur Gears

Avil Allwyn Dsa[1*], Helga Lobo[2], AR Rajesh [3], Joseph Gonsalves[4]

[1] Department of Mechanical Engineering, Don Bosco College of Engineering, Goa, India
[2] Department of Computer Science and Engineering, National Institute of Technology, Goa, India
[3] Department of Mechanical Engineering, Government Polytechnic, Kushalnagar, Karnataka, India
[4] Former Professor, Principal & Research Advisor, St Joseph Engineering College, Mangalore, Karnataka, India

ARTICLE INFO

Article history:
Received: 30/09/2025
Revised: 26/08/2026,
Accepted: 12/09/2026
Available online: 15/09/2026.

Keywords:
Gear root fillet
Altered tooth-sum gears
Profile shift
ISO 6336-3
Cutter kinematics

ABSTRACT

The strength of a gear tooth is strongly influenced by its root fillet, where cracks can initiate under repeated loading. Accurate representation of this region is therefore essential for reliable stress prediction. However, design standards such as ISO 6336-3 represent the root fillet using simplified circular approximations rather than the exact cutter-generated geometry. While adequate for standard gears, these approximations may become less representative when substantial profile shifts are introduced, particularly in Altered Tooth-sum Gears (ATG), where systematic profile shifts enable tooth-sum modification while maintaining the prescribed centre distance. This study develops a cutter-tool-path-based analytical formulation for the ATG root fillet. The formulation is first validated geometrically against a simulated cutter envelope, then compared with the ISO 6336-3 circular approximation, and a controlled finite-element analysis is performed to isolate the influence of fillet geometry on tooth-root stress. For a representative ATG configuration, the critical-section thickness deviation from the ISO representation increases from approximately 6% to 12.47% with increasing negative profile shift. The corresponding maximum root stress is approximately 332 MPa for the analytically generated fillet, compared with 443 MPa for the ISO circular approximation, representing a difference of approximately 25%. These results show that, for ATG configurations with substantial profile shifts, the ISO circular approximation can significantly overpredict root stress, underscoring the need for cutter-generated fillet geometry in their design evaluation.

1. INTRODUCTION

The gear root fillet is one of the most critical regions of a gear tooth because it governs bending strength and is the location most susceptible to fatigue failure under cyclic loading. For this reason, an accurate description of the fillet geometry is essential in both analytical and numerical stress evaluations. ISO 6336-3 [1] provides specific procedures in clauses 6.2.3 to 6.2.5 for calculating the equivalent root fillet radius, the tooth root normal chord, and the bending moment arm. Although these standardized geometric quantities do not explicitly reconstruct the complete cutter-generated fillet profile, they provide a convenient and effective engineering approximation for bending-stress evaluation in standard gears. In recent years, non-standard gear methodologies, such as Altered Tooth-sum Gearing (*ATG*) [2], have gained attention because of the additional flexibility they offer in gear design. Such approaches employ deliberate modifications of conventional gear geometry, including profile shifts, which alter the relative geometry between the generating tool and the gear and can consequently affect the resulting root-fillet profile. Consequently, the direct application of conventional ISO root-fillet representations to these configurations warrants careful consideration.

A number of studies have investigated bending-stress behavior in both standard and non-standard spur gears using analytical, numerical, and standards-based approaches. Mouton et al. [3] and Pedrero et al. [4] adopted ISO-based approaches or introduced modification factors in their investigations of spur-gear root stresses, and Bonaiti et al. [5] similarly proposed a fatigue-limit-based correction to the constant factor

*Corresponding author's E-mail: avil.dsa@dbcegoa.ac.in | ORCID: 0000-0002-7728-3921
DOI: 10.24237/djes.2026.19308

conventionally used to translate single-tooth bending fatigue results into full meshing-gear ratings under ISO 6336. Similarly, studies of *ATG* by Rajesh and Gonsalvis have employed ISO-style circular fillet representations to examine bending stress under static loading [6] and load sharing along the path of contact [7], and validated *ATG* bending-stress predictions experimentally using a strain-gauged single-tooth Gear Tooth Bending Test fixture benchmarked against AGMA [8]. Krishnamurthy and Kurkal [9] similarly compared four rack-cutter tip geometries without deriving the fillet from the tool path itself. Studies on root fillet and bending-stress analysis using commercial CAD packages [10, 11] typically generate fillets using default blending arcs, which may not reproduce the actual geometry generated by the cutting tool. Other investigations have pursued gear performance improvements through broader geometric-parameter optimization [12] and finite-element evaluation of bending and contact strength under machining and assembly errors [13], while asymmetric tooth geometries have been explored to reduce root stress concentration through altered flank symmetry [14, 15]. As with the ISO- and CAD-based approaches above, these studies rely on prescribed or simplified root-fillet representations rather than one derived from the generating tool path.

Beyond these standards- and geometry-based approaches, analytical methods have also been developed to describe cutter-generated root profiles. Litvin's vector-based meshing-equation formulation [16] provides the general kinematic foundation for deriving such tooth and fillet surfaces directly from cutter motion, and Fetvaci and Şentürk [17] recently applied this approach to derive the rack-cutter-generated locus in the transverse section. Spitas and Spitas [18] investigated the effect of enlarged cutter tip radius on trochoidal root fillet strength, directly modifying the fillet geometry itself rather than treating it as fixed, while Dong et al. [19] investigated modified tooth-root profiles generated through hobbing using a Bézier-defined hob-tip contour. A recent geometric reassessment [20] further clarifies that the cutter-generated fillet is genuinely trochoidal only for pinion-shaped cutters, whereas for rack-type cutters — the case considered throughout this work — the exact locus generated is a prolate involute rather than a trochoid. These studies demonstrate that the root geometry produced by the generating tool can be explicitly modelled rather than represented solely by a conventional blending curve. However, the reported analytical treatments have primarily considered conventional gear-generation configurations, with profile shift, where present, treated as a moderate and freely chosen design parameter rather than one constrained by a fixed center distance, and none address the large, systematic profile shifts imposed by tooth-sum alteration.

Thus, although extensive research has addressed root-fillet geometry and bending performance for standard and non-standard spur gears, the accuracy of stress prediction ultimately depends on the fidelity with which the root region is represented, irrespective of the analysis approach employed. While ISO-based root fillet approximations are well suited to standard gears, the cutter-generated root-fillet geometry associated with systematic profile shifts in *ATG* remains insufficiently characterized, since the geometric changes *ATG* introduces can alter the actual root profile relative to the conventional ISO representation. This observation motivates the development of root fillet profiles derived directly from the cutter tool-path to achieve higher geometric fidelity for such configurations.

Specifically, the research gap addressed in this work is the absence of a cutter-kinematics-based analytical formulation for the root fillet of *ATG*. Existing cutter-generated fillet formulations [16–20] have been developed mainly for standard or moderately shifted gears, whereas existing *ATG* studies [6–9, 21] rely on ISO-style or otherwise simplified fillet representations. The objective of this study is therefore to extend cutter kinematics theory to the *ATG* framework and develop a tool-path-based analytical formulation of the root fillet, and to quantify the resulting geometric deviation from the ISO 6336-3 circular approximation. This study makes three original contributions relative to existing cutter-based, ISO-based, and numerical gear-modelling approaches. First, it provides a unified closed-form description of the root fillet and conjugate involute flank for *ATG*. Second, it quantifies the range over which the ISO 6336-3 circular approximation remains acceptable for *ATG*. Third, it provides a controlled finite-element comparison that isolates the effect of fillet geometry on tooth-root stress and links the resulting geometric deviation to its mechanical consequence.

2. BACKGROUND

2.1 Gear geometry modification by tooth-sum alteration

From classical gear theory [22, 23], the pitch circle radius of a spur gear is directly proportional to its center distance and inversely proportional to the total number of teeth of the mating pair. Altering the tooth-sum while maintaining an invariant center distance consequently modifies the effective meshing pitch circles and the operating pressure angle. A reduction in the total tooth-count leads to enlarged tooth spaces, whereas an increase requires a corresponding reduction in tooth thickness to accommodate the additional teeth. Profile shifting is a gear design technique that modifies tooth thickness and tooth space distribution along the tooth profile without altering the number of teeth. When applied appropriately, profile shifting allows the restoration of conjugate action disrupted by tooth-sum alteration by introducing a calculated total profile shift proportional to the altered tooth sum.

In a gear drive, a fixed center distance can accommodate a wide range of tooth sums and gear ratios. The module m mainly controls load capacity, while the tooth-sum sets the transmission ratio and output speed. In a standard pair with reference tooth-sum z_s^r, the operating pressure angle ϕ_{w} and center distance c_w are identical to the standard pressure angle ϕ_{p} and center distance c_s^r. If the tooth sum is altered by a tooth-sum alteration factor $TAF\ \alpha$, such that $z_s^a = \alpha z_s^r$, and the centre distance is modified by a center-distance alteration factor $CAF\ \beta$, such that $c_w^a = \beta c_s^r$, then it can be shown that the relation between standard and the operating pressure angle (ϕ_p, ϕ_w) and pitch circles (r_p, r_w), as illustrated in Figure 1, can be expressed as [2]:

$$\left(\frac{\cos\phi_w}{\cos\phi_p}\right) = \frac{r_p}{r_w} = \frac{\alpha}{\beta} \tag{1}$$

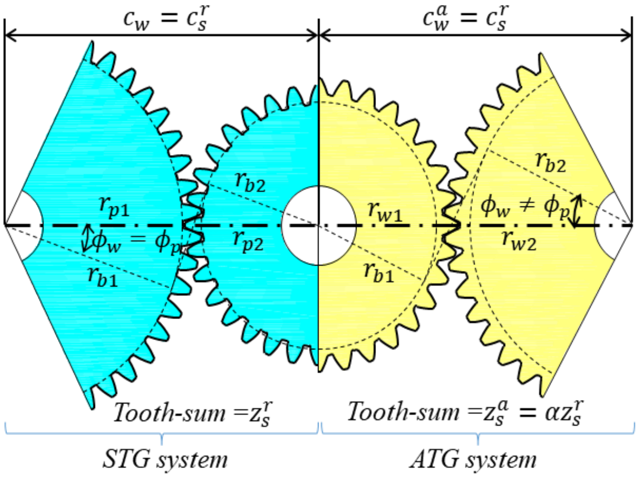

Figure 1. Geometric comparison Standard tooth-sum gear and ATG system. Adapted from [24]

Using the operating pressure angle obtained from Eq.(1), the module-normalized Total Profile Shift Coefficient $TPSC\ X_s$, [2] required to satisfy the conjugate meshing condition is determined from:

$$X_s = \left(\frac{m z_s^a \left(inv\phi_w - inv\phi_p\right) - B\alpha}{2m\beta \tan\phi_p}\right) \tag{2}$$

The $TPSC\ X_s$, must be distributed between the pinion and the gear. If x_1 and x_2 denote the profile shift coefficients of the pinion and the gear, respectively, then for analytical formulation the $TPSC\ X_s$ is defined as:

$$X_s = x_1 + x_2 \tag{3}$$

A tooth topping coefficient $TTC\ Y$ [2] that ensures adequate root clearance in ATG and other non-standard gears is given by:

$$Y = X_s + \left(\frac{Z_s^r}{2}\right)(\alpha - \beta) \tag{4}$$

The ratio of profile shift coefficient x_1 on the driver to that of the $TPSC\ X_s$, for a gear-pair is defined as the profile shift factor κ [2]. This ratio, which distributes the total profile shift between the mating gears, is given by:

$$\kappa = \left(\frac{x_1}{X_s}\right) \tag{5}$$

Eqs. (1) to Eq. (5) are a set of general expressions suitable for standard and non-standard spur gears. For a standard tooth-sum gear-pair (STG), $\alpha = \beta = 1$. For the ATG system, $0.96 < \alpha < 1.04$ and $\beta = 1$. For the S± profile shifted system, $0.96 < \beta < 1.04$ and $\alpha = 1$. These relationships establish the fundamental dependence of operating pressure angle, profile shift, and tooth topping on $TAF\ \alpha$, and $CAF\ \beta$.

The geometric framework underlying these governing equations has been developed in earlier work on ATG [2, 21, 24] and non-standard gears in general [22]. Accordingly, only the essential relations required for the present analysis are summarized here, while interested readers are referred to the cited publications for detailed derivations and comprehensive geometric discussion.

2.2 ISO Standard Recommendation for Root Fillet Radius

The basic reference rack specified in ISO 21771:2007 [25] is illustrated in Figure. 2.

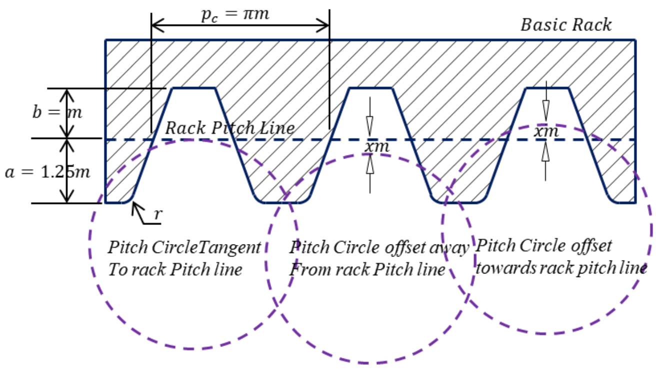

Figure 2. Rack proportions and profile shift (Zero, positive and negative), per ISO 21771:2007 [25]

The rack pitch line coincides with the gear pitch circle in the standard case, while positive or negative profile shifts displace the gear pitch circle relative to this line. The ISO 6336-3 treatment of the root region provides an analytical expression [1] for an equivalent circular fillet radius, ρ_f to be used at the critical section for bending-strength calculations.

$$\rho_f = r + m\frac{2G^2}{\cos\theta\left(z\cos^2\psi - 2G\right)} \tag{6}$$

where m is the module, r is the tool tip radius of the generating cutter, z is the tooth count, ψ is the critical-section tangent angle (typically 30deg for external gears), and G is a geometry term that condenses the generating data of the basic rack (addendum, clearance, profile shift, etc.).

$$G = \frac{r}{m} - \frac{a}{m} + x \tag{7}$$

Where $a = 1.25m$ is the addendum height of the rack and ‘x’ is the profile shift coefficient (Refer Figure. 2). The fillet radius from Eq. (6) provides a single radius that is consistent with ISO’s bending form factor and stress correction factor calculations.

While ISO 6336-3 recommendations provide a widely accepted framework for gear design and strength assessment, particularly for standard gear systems, the equivalent circular fillet representation is intended primarily for simplified stress evaluation rather than for describing the generated root fillet geometry. When applied to non-standard gears, where the root fillet geometry deviates significantly from standard forms, the circular fillet assumption may not adequately capture the true generated root shape, which can affect the accurate evaluation of both the magnitude and location of critical root stresses. In this context, the cutter–gear kinematics-based formulation presented in Section-3 provides an analytical description of the generated root fillet geometry, which forms the basis for evaluating the magnitude and location of critical root stresses in *ATG* and other non-standard spur gears.

3. CUTTER KINEMATIC-BASED ROOT FILLET EQUATION

To address the limitations associated with equivalent circular fillet representations when modelling non-standard gear geometries, this section presents a root fillet formulation derived from cutter–gear kinematics. The root fillet is described as the locus traced by the rack cutter tip during the generation process, consistent with the fundamental principles of involute gear generation. The formulation explicitly accounts for cutter geometry, profile shift, and the relative rolling motion between the cutter and the gear, and provides a systematic means for determining the generated root fillet geometry in *ATG* and other non-standard spur gears.

Two cartesian coordinate frames (Refer Figure. 3) are introduced to describe the relative motion. Frame $\{1\}$ is rigidly attached to the rack cutter, with its origin located at point M. Frame $\{2\}$ is fixed at the gear, with its origin at the pitch point P, where the rack pitch line coincides with the gear pitch circle. The pitch point thus provides an invariant reference for describing both the translational motion of the cutter and the resulting fillet geometry.

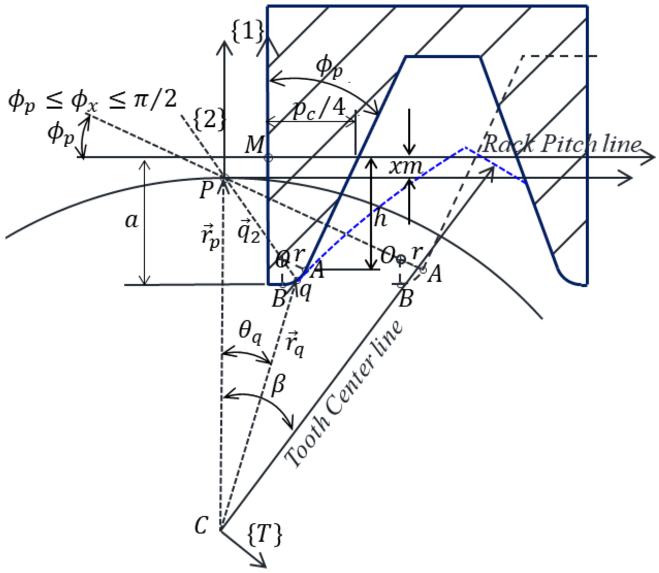

Figure 3. Cutter kinematic-based root fillet generation

The rack cutter is characterized by its addendum a, circular tip radius r, standard pressure angle ϕ_p, and circular pitch p_c. During the generation process, the cutter undergoes pure translational motion relative to the gear, while the gear executes a corresponding rolling rotation to satisfy the no-slip condition at the pitch point. The generated root fillet is obtained as the locus of the instantaneous cutting point traced during this combined translational–rolling motion.

The normality condition requires that the normal at the active cutter point passes through both the fillet center and the pitch point. Consequently, the cutting point always lies on the extension of the line PO, and its position is uniquely determined once the cutter center location is known. This constraint applies uniformly throughout the generation process and is valid for the lower limiting point B, any intermediate contact point q, and the upper limiting point A. At the lower limit of fillet generation, the active cutter point B and the cutter center O lie directly below the pitch point P. In the gear-fixed frame $\{2\}$, this geometric condition gives:

$$O_{2x} = B_{2x} = 0 \tag{8}$$

The upper limit of fillet generation is governed by point A, corresponding to the configuration at which the cutter point reaches the top of the generated fillet. At this position, the vertical displacement of the cutter-fixed frame $\{1\}$, expressed in the gear-fixed frame $\{2\}$, equals the prescribed cutter offset, yielding:

$$M_{2y} = xm \tag{9}$$

The relationship between the cutter position, the fillet center, and the limiting points of the generated root fillet provide the foundation for deriving the complete locus of fillet points. The valid range of motion is bounded by the condition $-\phi_p \le \phi_x \le -\pi/2$, which corresponds to the cutter sweeping from the uppermost contact at point A to the lowermost contact at point B.

Once the limiting positions have been defined, the intermediate points of the fillet are obtained by varying the angular position ϕ_x of the cutter center. By dividing this interval into sufficiently small increments, a sequence of cutter positions can be determined, each producing a distinct point on the fillet curve. For a given cutter position, the Cartesian coordinates of the fillet center 'O' in frame {1} are given by

$$\begin{cases} O_{1x} = B_{1x} = \left(\dfrac{p_c}{4} - h\tan\phi_p - r\cos\phi_p\right) \\ O_{1y} = -(a-r) \end{cases} \quad (10)$$

The parameter h denotes the vertical distance measured from the rack pitch line to point A, where point A is the tangency point between the inclined rack flank at the standard pressure angle ϕ_p and the circular fillet of radius r at the cutter tip. This distance is determined solely by the rack geometry and is given by:

$$h = \left(a - r + r\sin\phi_p\right) \quad (11)$$

Since the cutter undergoes only translational motion, the transformation from the cutter-fixed frame {1} to the gear-fixed frame {2} is accomplished by simple vector addition. The cutter center coordinates in Frame {2} are therefore:

$$O_{2x} = O_{1x} + M_{2x},\ O_{2y} = O_{1y} + M_{2y} \quad (12)$$

Fillet generation under the normality condition requires the common normal at the cutting point to pass through both the fillet center O and the pitch point P. Thus, the line PO defines the normal direction and is inclined at an angle ϕ_x with respect to the horizontal axis of the gear-fixed frame {2}. This inclination of the normal yields the following relationship between the Cartesian coordinates of the cutter center O in frame {2}:

$$O_{2x} = \frac{O_{2y}}{\tan\phi_x} = \frac{O_{1y} + xm}{\tan\phi_x} \quad (13)$$

Combining the coordinate transformation in Eq. (12) with Eq. (13), and substituting the cutter center coordinates from Eq. (10), the horizontal displacement of the cutter is obtained as:

$$M_{2x} = \left[\left(\frac{O_{1y} + xm}{\tan\phi_x}\right) - \left(\frac{p_c}{4} - h\tan\phi_p - r\cos\phi_p\right)\right] \quad (14)$$

Where ϕ_x is the angular position of the cutter center relative to the pitch point. The distance from the cutter center O to pitch point P can be expressed as:

$$PO = \sqrt{O_{2x}^2 + O_{2y}^2} \quad (15)$$

By definition, the cutting point lies on the extension of the line PO, at a distance equal to the cutter radius beyond the center. Therefore, the distance from the pitch point P to any arbitrary point q on the cutter fillet between A and B can be expressed as:

$$Pq = PO + r \quad (16)$$

Since the cutting point lies on the extension of line PO, the coordinates of the point q in frame {2} are then determined through proportional scaling along this line:

$$q_{2x} = \frac{Pq}{PO} \times O_{2x},\ q_{2y} = \frac{Pq}{PO} \times O_{2y} \quad (17)$$

Referring the vector loop CPq in Figure. 3, the instantaneous location of the arbitrary cutter point q, expressed with respect to the gear center C is given by:

$$\begin{cases} r_q = \sqrt{(q_{2x})^2 + (r_p + q_{2y})^2} \\ \theta_q = \tan^{-1}\left(\dfrac{q_{2x}}{r_p + q_{2y}}\right) \end{cases} \quad (18)$$

The term $r_p + q_{2y}$ is the instantaneous vertical offset of the cutting point relative to the gear center. Together with the horizontal component q_{2x}, it defines the radius vector $\vec{r}_q$ from the gear center to the cutting point.

During generation, the rack translates along the pitch line while the gear rolls without slip on its pitch circle. If M_{2x} denotes the horizontal displacement of the rack reference point in frame {2}, then the associated rigid-body rotation of the gear, β (used here to denote this rolling rotation angle, distinct from the $CAF\ \beta$ of Section 2.1) and hence of the tooth center line is given by:

$$\beta = \left(\frac{(M_{2x} + p_c/2)}{r_p}\right) \quad (19)$$

The constant term $p_c/2$, representing one-half of the circular pitch measured along the pitch line, accounts for the relative phase alignment between the gear tooth center line and the rack reference position.

In the gear tooth reference frame $\{t\}$, the position of the point X on the generated root profile, which coincides instantaneously with the cutter point q, is described by the polar coordinates (r_x, θ_x) given by:

$$\begin{cases} r_x = r_q \\ \theta_x = \theta_q - \beta \end{cases} \quad (20)$$

where r_q and θ_q denote the instantaneous polar coordinates of the cutting point q relative to the gear center, and β represents the rigid-body rolling rotation of the gear. The corresponding Cartesian coordinates in the tooth reference frame $\{t\}$ follow as:

$$x = r_x\sin\theta_x\ ,\ y = r_x\cos\theta_x \quad (21)$$

By continuously varying the cutter angular position ϕ_x

within the admissible range, the complete locus of the gear root fillet is obtained. The resulting curve represents the true kinematic path traced by the rack cutter tip during manufacture, fully accounting for both translational and rolling components of motion.
The extremal radial positions of this locus define the limiting geometry of the root region. The maximum radial distance corresponds to the fillet circle, whereas the minimum radial distance corresponds to the root circle. Accordingly, the fillet circle radius [23] is obtained as:

$$r_f^2 = r_b^2 + \left[r_b \tan\phi_p - \left(\frac{h - xm}{\sin\phi_p} \right) \right]^2 \tag{22}$$

Eq. (22) defines the fillet circle associated with the limiting cutter configuration, completing the analytical description of the generated root geometry based on cutter–gear kinematics. With the root fillet formulation established, the involute portion of the tooth profile is developed in the following section.

4. INVOLUTE PROFILE FOR *ATG*

An accurate representation of involute tooth geometry and simulation of gear generation by a rack cutter constitute the foundation for modeling both the tooth flanks and the root fillet of standard spur gears (STG) and *ATG*. Any admissible tooth form must satisfy the fundamental law of gearing, which requires that the common normal at the point of contact intersect a fixed pitch point on the line of centers, thereby ensuring a constant angular-velocity ratio between the mating gears. A generalized mathematical formulation, whether with or without profile shift, should therefore satisfy the following conditions: **a)** The distance between the coordinate system origins of the two gears is constant. **b)** The angular-velocity ratio between the gears of a gear pair is constant. **c)** The components of the velocity vectors along the common normal at the point of mesh are equal.
When these kinematic conditions are combined with a rack-cutter generation model, the resulting formulation provides the parametric description of both standard and non-standard gear geometries, including *ATG*, while ensuring compliance with the governing law of gearing. The expressions for the generation of involute curves are available in classical texts on gear geometry [22, 23]. However, these relations are not expressed in a form that explicitly enforces the conjugacy and center-distance constraints governing a meshing gear pair. Closed vector-loop relationships, matrix representations and coordinate transformation are well established tools in mechanism kinematics and have also been applied in gear geometry modeling [16]. In the present formulation, these concepts are employed to obtain the coordinates of the corresponding contact points on the mating gears using a closed vector-loop relationship between the rotating coordinate frames attached to the pinion and the gear. The resulting formulation provides a computationally convenient framework for determining the coordinates of the meshing gear pair while satisfying the conjugacy condition for a given center distance.
A rotating coordinate frame {1} and {2} are rigidly attached to the pinion and the gear, respectively, as shown in Figure. 4. The constant position between frame {1} and {2}, representing the center distance, is denoted by c_w. The global frame is denoted by {G} and the roll angles of the pinion and the gear are denoted by θ_1 and θ_2, respectively. By definition, the circles on the pinion and the gear that locate the start and end point of mesh are referred to as the limiting circles. If it is assumed that the contact starts at $s = 0$ when the roll angle $\theta_1 = 0$, then the roll angle at which the contact starts and ends is given by:

$$\theta_{1s} = \left(\frac{\rho_{l1}}{r_{b1}} \right);\ \theta_{1e} = \left(\frac{\rho_{a1}}{r_{b1}} \right) \tag{23}$$

Where ρ_l & ρ_a represents the radius of curvature corresponding to limit and addendum circles.

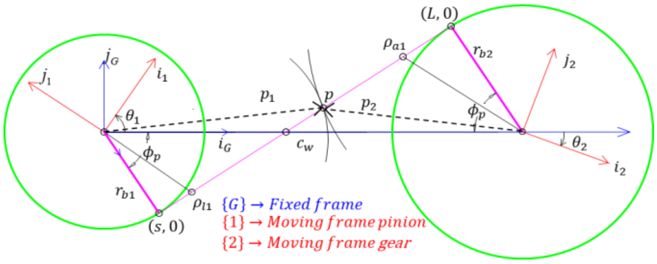

Figure 4. Closed position vector loop

If the surfaces of two gears are in contact at some point *p,* then the position vector of point relative to frame {1} is p_1 and, p_2 is the position vector of point P relative to frame {2}. The position vector p_1 in the global frame of reference {G} can be expressed as:

$$[\vec{p}_1]_G = [\vec{r}_{b1}]_G + [\vec{\rho}_p]_G \tag{24}$$

Transforming the description of p_1 from global reference frame $\{G\}$ to local frame {1} using direction cosine transformation matrix corresponding to rotation θ_1 gives:

$$\begin{Bmatrix} p_{1x} \\ p_{1y} \end{Bmatrix}_1 = \begin{bmatrix} \cos\theta_1 & -\sin\theta_1 \\ \sin\theta_1 & \cos\theta_1 \end{bmatrix}_G^{1} \times \begin{bmatrix} r_{b1}\cos\phi_p + r_{b1}\theta_1 \sin\phi_p \\ -r_{b1}\sin\phi_p + r_{b1}\theta_1\cos\phi_p \end{bmatrix}_G \tag{25}$$

For the gear tooth pair to satisfy the condition of conjugate action, the loop-closure equation must be satisfied at all instants of time. The closed position vector loop equation is given as:

$$\vec{p}_2 = \vec{p}_1 - \vec{c}_w \tag{26}$$

Expressing the above vector equation in terms of its components in local and global frames gives:

$$\begin{bmatrix} \hat{i} & \hat{j} \end{bmatrix}_2 \begin{Bmatrix} p_{2x} \\ p_{2y} \end{Bmatrix}_2 = \begin{bmatrix} \hat{i} & \hat{j} \end{bmatrix}_1 \begin{Bmatrix} p_{1x} \\ p_{1y} \end{Bmatrix}_1 - \begin{bmatrix} \hat{i} & \hat{j} \end{bmatrix}_G \begin{Bmatrix} c_w \\ 0 \end{Bmatrix} \tag{27}$$

The local-to-global transformation matrix [16] is used to eliminate the unit vectors, yielding:

$$\begin{bmatrix} l_1 & l_2 \\ m_1 & m_2 \end{bmatrix}_2^G \begin{Bmatrix} p_{2x} \\ p_{2y} \end{Bmatrix}_2 = \begin{bmatrix} l_1 & l_2 \\ m_1 & m_2 \end{bmatrix}_1^G \begin{Bmatrix} p_{1x} \\ p_{1y} \end{Bmatrix}_1 - \begin{Bmatrix} c_w \\ 0 \end{Bmatrix}_G \tag{28}$$

where *l* and *m* are the direction cosines of the respective local axes with respect to the global frame. Solving for the coordinates of position vector p_2 gives:

$$\begin{Bmatrix} p_{2x} \\ p_{2y} \end{Bmatrix}_2 = \begin{bmatrix} \cos(\theta_1+\theta_2) & -\sin(\theta_1+\theta_2) \\ \sin(\theta_1+\theta_2) & \cos(\theta_1+\theta_2) \end{bmatrix}_1^2 \times \begin{Bmatrix} p_{1x} \\ p_{1y} \end{Bmatrix}_1 - \begin{bmatrix} \cos\theta_2 & -\sin\theta_2 \\ \sin\theta_2 & \cos\theta_2 \end{bmatrix}_G^2 \begin{Bmatrix} c_w \\ 0 \end{Bmatrix}_G \tag{29}$$

The expressions derived in Eqs. (8)-to-(21), together with Eqs. (25) and (29), are used to model the root fillet and tooth profile of the *ATG*.

5. INVESTIGATION METHODOLOGY

A reference gear pair of module $m = 3\ mm$, tooth-sum $z_s^r = 80$, and pressure angle $\phi_p = 20°$ transmitting power between a center distance $c_w = 120\ mm$ is altered with *TAF* $\alpha = 1.0375$ and *TAF* $\alpha = 0.975$ for this case study. The calculation of the *ATG* geometry modification parameters, as described in Section 2.1 and Eqs. (1)-to-(5) are presented in Table 1. The total shift X_s is shared between the pinion and the gear using the profile shift factor κ. The dimension of the root fillet as per the ISO recommendation is calculated using Eq. (6) and Eq. (7) and tabulated in Table 2.

Table 1. *ATG* Geometrical Parameters

$m = 3\ mm$, $z_s^r = 80$, $\phi_p = 20°$, $\beta = 1$ and $B = 0$

α	$z_s^a = \alpha z_s^r$	z_1	ϕ_w (Rad)	X_s	Y
0.975	78	39	0.4122	1.089	0.089
1	80	40	0.349	0	0
1.0375	83	40	0.2242	-1.261	0.239

Table 2. ISO Root fillet Radius

$m = 3\ mm,\ z_s^r = 80,\ \phi_p = 20°,\ \beta = 1,\ r = 0.25m,\ a = 1.25m$

α	z_s^a	z_1	κ	x_1	G	ρ_f
0.975	78	39	0.5	0.5445	-0.455	0.8mm
			0.2	0.2178	-0.782	0.89mm
1.0375	83	40	0.25	-0.315	-1.312	1.12mm
			0.5	-0.6305	-1.63	1.3mm
			0.75	-0.945	-1.94	1.52mm

The flow chart of the computational routine implementing Eqs. (8)–(21) is presented in Figure. 5.

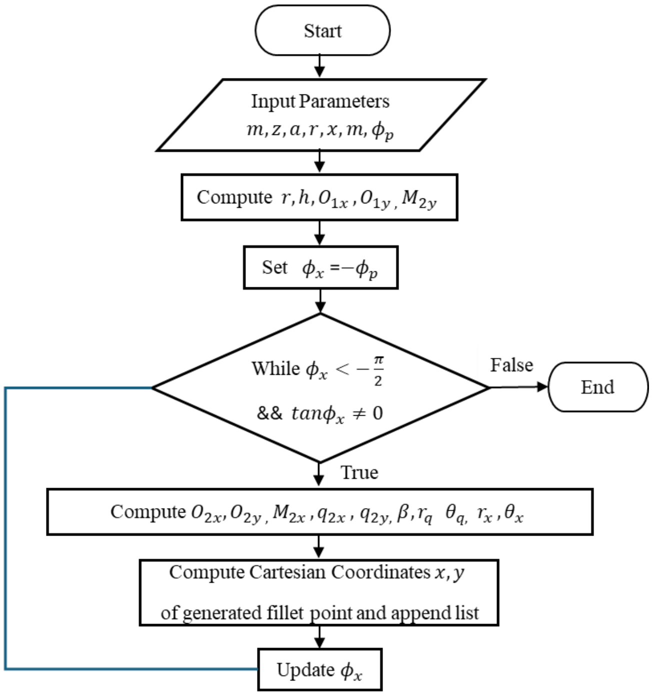

Figure 5. Fillet coordinate routine

The complete tooth profile, comprising the analytically generated root fillet and involute (Eqs. (23) and (29)), is computed parametrically in MATLAB (*MathWorks Inc., USA*) through direct evaluation of the governing equations. For numerical generation of the fillet and tooth profiles, the cutter angular position was varied incrementally in steps of 0.5°. The resulting ordered coordinate set is exported as an AutoCAD script (.scr) file, which is executed within AutoCAD Mechanical (*Autodesk Inc., USA*) to reconstruct the continuous tooth geometry via spline interpolation. The resulting gear tooth wireframe models of *ATG*, incorporating analytically generated root fillets for different profile shift coefficients, are compared with the corresponding *ATG* models employing ISO-recommended circular root fillets in order to evaluate the profile deviations in the root region. To demonstrate the consequences of root fillet profile deviations on the tooth root stress in *ATG*, a comparative evaluation between gears incorporating true cutter-path-based fillet and those employing approximate ISO-based circular fillets is necessary.

According to ISO 6336-3, the tooth root bending stress is evaluated using the form factor Y_F, which depends on the geometry of the critical section defined by the tooth root normal chord. Within the present analytical formulation, the coordinates of the critical section can be identified as the point on the fillet curve where the local slope satisfies $dy/dx = \tan 60 = 1.732$. Twice the absolute value of the x-coordinate provides the dimension and y-coordinate defines the location of the critical section relative to the gear centre.

However, no standardized analytical framework comparable to the ISO formulation is available for determining form factors of teeth incorporating analytically generated non-circular fillets. Furthermore, substituting the critical section dimensions obtained from analytically generated non-circular fillets directly into the ISO form factor equation is not appropriate, since the ISO parameters are fundamentally designed for circular root fillet geometries. Therefore, finite element analysis (FEA) is adopted in the present study as a geometry-independent evaluation framework.

The gear tooth wireframe models are exported from AutoCAD Mechanical in IGES format and imported into MSC Patran/Nastran (*Hexagon AB, Sweden*) for FEA. The wireframe geometries are first converted into surface models within MSC Patran. The bounding curves are discretized using the mesh seeding option to control element density along the geometry. The surfaces are meshed with 4-node linear quadrilateral (Quad4) and 3-node linear triangular (Tria3) shell elements, generated using the automatic hybrid surface mesher available in MSC Patran. A linear-elastic steel material model was assigned, with Young's modulus $E = 206GPa$ and Poisson's ratio $\nu = 0.3$.

The FEA is based on a plane stress condition across the face width, with the shell thickness of 1mm representing a unit face width of the gear tooth. The model is considered as an isolated tooth segment, and the base region is fully constrained to represent the stiffness of the gear body, while the remaining surfaces are left traction-free. A normal load of 300 N/mm (per unit face width) was applied at a radius of 60 mm, slightly below the tooth-tip boundary, to avoid direct tip loading, and was directed normal to the involute flank. The same load magnitude, direction, and application location were used for both the analytically generated and ISO circular root-fillet models. The maximum von Mises stress in the tooth-root region was used as the stress measure for comparison between the analytically generated and ISO-based fillet geometries.

A mesh convergence study was conducted using progressively refined shell meshes. The maximum root stress increased from 440 MPa to 443 MPa when the element count was increased from 1843 to 4178, corresponding to a variation of less than 1%. The negligible change in stress with further refinement confirms that the mesh is sufficiently converged for accurate stress evaluation.

Element count	Element type	Fillet stress (Mpa)	Convergence assessment
1843	Quad4 2D-shell	440	Coarse mesh
3637	Quad4 2D-shell	442	0.45% increase from previous mesh
4178	Quad4 2D-shell	443	0.23% increase-converged

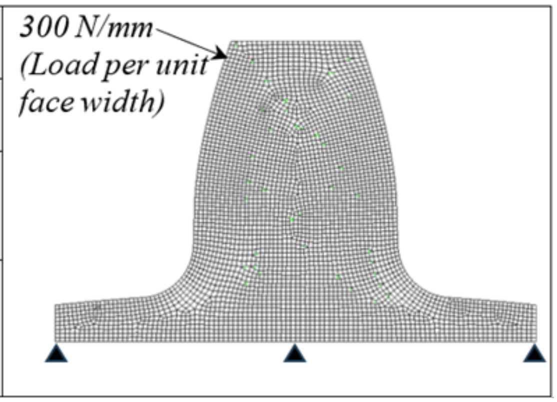

Figure 6. FEA Loading, Boundary & Convergence

Table 3. Profile deviation at critical section

Standard gear of $\boldsymbol{m = 3\ mm}$, $\boldsymbol{z_s^r = 80}$, $\boldsymbol{\phi = 20}$°, and $\boldsymbol{\beta = 1}$							
$\boldsymbol{\alpha}$	$z_s^a = \alpha z_s^r$	z_1	x_1	ρ_f(mm)	t_{iso}	t_{actual}	% Deviation
0.975	78	39	0.2178	0.89	6.51	6.59	1.2%
0.975	78	39	0.5445	0.8	6.91	6.94	0.43%
1.0375	83	40	-0.315	1.12	5.67	6.01	6.0%
1.0375	83	40	-0.6305	1.3	5.13	5.60	9.16%
1.0375	83	40	-0.945	1.52	4.65	5.23	12.47%

6. RESULTS AND DISCUSSION

The derived formulation was applied to *ATG* to evaluate its capability to reproduce the generated root fillet geometry. A standard rack of module $m = 3$ mm, pressure angle $\phi_p = 20°$, addendum coefficient equal to unity, and rack tip radius $r = 0.25m$ was considered. The governing equations were implemented in a numerical routine to compute the locus of fillet points traced by the rack cutter tip for two ATG configurations with $TAF\ \alpha = 0.975$ and $TAF\ \alpha = 1.0375$ and different profile shifts. The analytical results were verified through comparison with simulated cutter envelopes and subsequently evaluated against the ISO-recommended circular root fillet approximation.

The analytically generated root fillet exhibits excellent agreement with the simulated cutter envelope (Figs. 7 and 8), confirming that the formulation accurately captures the kinematics of rack cutter generation.

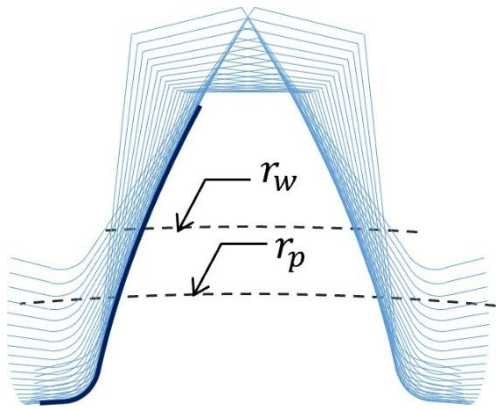

Figure 7. Root Envelope: Analytical vs. Simulation $TAF\ \alpha = 0.975\ z_1 = 39$

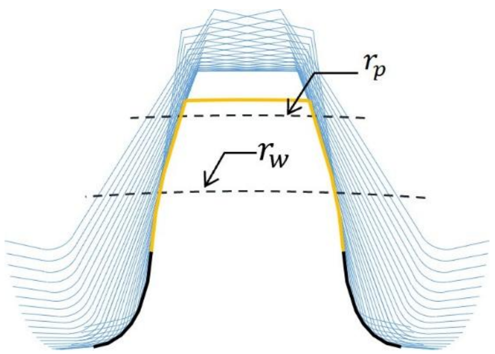

Figure 8. Root Envelope: Analytical vs. Simulation $TAF\ \alpha = 1.0375\ z_1 = 40\ x_1 = -0.6305$

A comparison with the ISO root fillet approximation shows that for ATG with $TAF\ \alpha = 0.975$, obtained using two different positive profile shifts, the ISO circular fillet closely matches the analytically generated root profile (Figure. 9 & 10), with the difference in critical section thickness remaining below 1.5% (refer Table. 3). This indicates that for negative tooth alteration achieved through positive profile shifts, the ISO approximation may provide a satisfactory representation. This behavior arises because a positive profile shift withdraws the rack cutter from the gear blank, reducing the depth of cutter engagement in the root region; the resulting fillet locus is swept through a shorter, more gently curving arc, which a single-radius circular approximation can represent with little error.

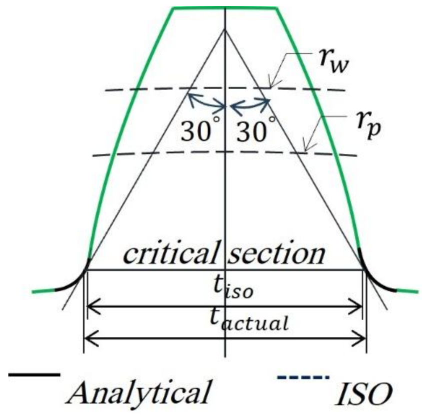

Figure 9. Root Envelope: Analytical vs. ISO $TAF\ \alpha = 0.975\ z_1 = 39\ x_1 = 0.2178$

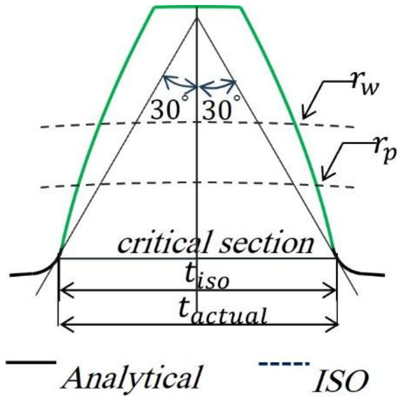

Figure 10. Root Envelope: Analytical vs. ISO $TAF\ \alpha = 0.975\ z_1 = 39\ x_1 = 0.5445$

For ATG with $TAF\ \alpha = 1.0375$, root profiles corresponding to three profile shift conditions were examined (Figs. 11–to-13). The deviation between the ISO and analytically generated fillets increases progressively with increasing negative profile shift magnitude. The largest differences occur in the upper root region near the critical section, where the ISO circular fillet exhibits lower curvature compared to the analytically generated root profile. This trend arises because a negative profile shift advances the rack cutter deeper into the gear blank, lengthening the cutter engagement path through the root region. The resulting fillet locus therefore sweeps through a wider range of local curvature from the root circle to the critical section, a variation that a single fixed-radius circular arc cannot represent, causing the discrepancy with the ISO approximation to grow as the negative shift magnitude increases.

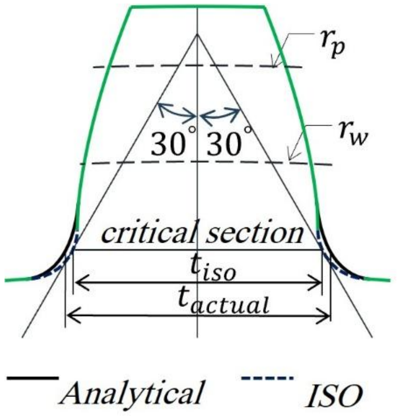

Figure 11. Root Envelope: Analytical vs. ISO $TAF\ \alpha = 1.0375\ z_1 = 40\ x_1 = -0.315$

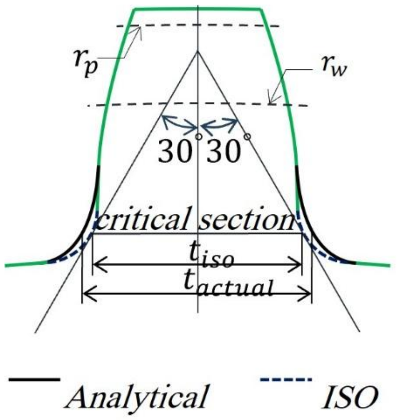

Figure 12. Root Envelope: Analytical vs. ISO $TAF\ \alpha = 1.0375\ z_1 = 40\ x_1 = -0.6305$

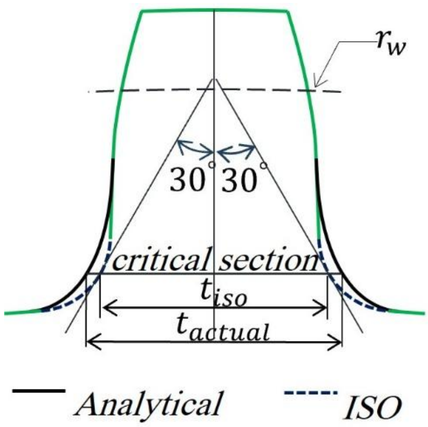

Figure 13. Root Envelope: Analytical vs. ISO $TAF\ \alpha = 1.0375\ z_1 = 40\ x_1 = -0.945$

The comparison of critical section thicknesses further highlights this effect. As shown in Table 3, the ISO-based thickness increasingly underestimates the actual thickness with increasing negative profile shift, with errors growing from approximately 6% to 12.5%. This monotonic increase in discrepancy indicates that the reliability of the circular approximation deteriorates progressively as the geometry deviates from standard conditions. The results therefore demonstrate that while the ISO approximation may be adequate for certain geometries, it becomes less representative for non-standard configurations such as *ATG*. Such deviations may lead to significant misestimation of tooth root stresses, potentially affecting gear strength assessment and design decisions.

A representative FEA of the root stress distribution for the *ATG* case with $TAF\ \alpha = 1.0375$, $z_1 = 40$, and $x_1 = -0.6305$ illustrates (Refer Figure. 14 & 15) the mechanical implications of the geometric differences between the analytically generated fillet and the ISO circular approximation. FEA is used as a controlled comparative assessment of the mechanical consequences of the differing root-fillet geometries on the predicted tooth-root stress, rather than as an independent validation of the absolute stress magnitudes. Both fillet representations are evaluated using identical material properties, loading, boundary conditions, and FEA formulation, thereby isolating the effect of the root-fillet geometry on the predicted tooth-root stress. The peak stresses on the loaded flank occur at the fillet critical section in both models. The maximum induced tooth root stress is approximately 332 MPa and 443 MPa for the two fillet representations under identical loading conditions, indicating an increase of about 25% when the ISO circular approximation is used.

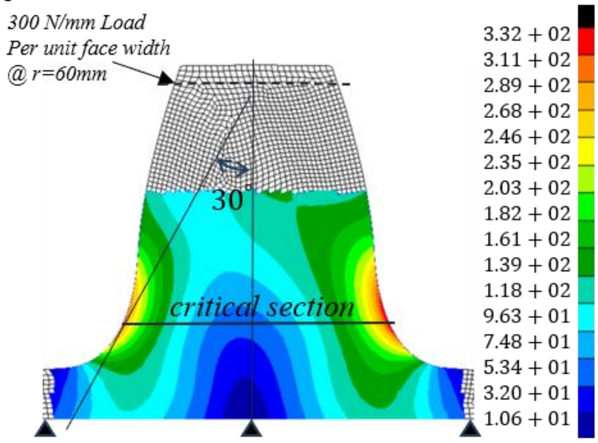

Figure 14. Root Stresses: Analytical Envelope $TAF\ \alpha = 1.0375\ z_1 = 40\ x_1 = -0.6305$

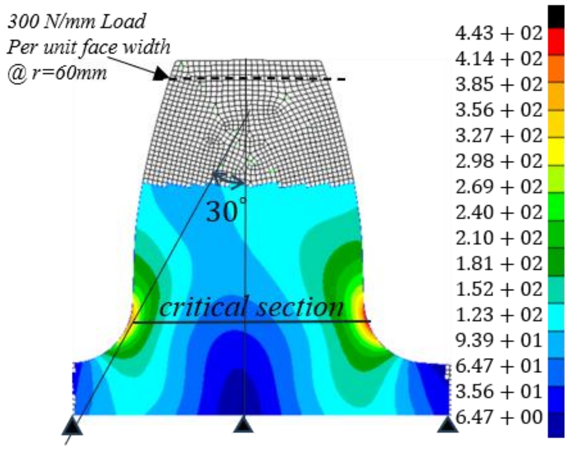

Figure 15. Root Stresses: ISO Envelope $TAF\ \alpha = 1.0375\ z_1 = 40\ x_1 = -0.6305$

The higher stresses obtained for the ISO circular fillet can be attributed to the reduced critical section thickness and smaller curvature radius associated with the circular representation. As the negative profile shift increases in ATG configurations, the circular approximation progressively underestimates the actual section thickness and produces a sharper curvature in the upper root region, thereby increasing the stress concentration at the fillet. In contrast, the analytically generated profile, obtained from the cutter tool path, provides a smoother curvature transition together with a larger effective load-carrying section, resulting in lower peak stresses.

The difference in stresses induced in the two fillet geometries becomes particularly important for non-standard ATG configurations, where cutter penetration alters the fillet formation mechanism. The higher stresses associated with the ISO circular representation indicate that reliance on the circular fillet may lead to conservative estimates of load-carrying capacity. While this provides additional safety margin, it may also result in underutilization of available material strength when the actual generated fillet deviates significantly from the circular assumption. Incorporating the analytically generated fillet geometry therefore provides a more realistic basis for stress evaluation and improves the reliability of strength assessment for gears with substantial negative profile modifications.

Overall, the results demonstrate that the proposed tool-path-based formulation accurately reproduces the cutter-generated root fillet and can be applied to any involute spur gear. Its use is particularly justified for ATG with negative profile shifts where higher geometric fidelity is needed to capture the true root profile. For ATG configurations with positive profile shifts, the ISO circular root fillet approximation generally remains adequate.

7. VALIDATION OF THE FEA-BASED STRESS COMPARISON

Both fillet representations in the present study were evaluated under identical material properties, loading, boundary conditions, and FEA formulation, isolating the effect of root-fillet geometry alone on the predicted stress. As a case-specific cross-check, the ISO circular fillet stress for the present case ($TAF\ \alpha = 1.0375$, $x_1 = -0.6305$, $z_1 = 40$) was independently computed using the classical fillet stress expression of Colbourne [23]:

$$\sigma_t^A = \frac{w}{m}\cos\gamma\left[K_f\left(\frac{1.5m\left(x_D - x_A\right)}{y_A^2}\right) - \left(\frac{0.5m\tan\gamma}{y_A}\right)\right] \tag{30}$$

where the stress-concentration factor K_f, obtained from the photo-elastic bending studies of Dolan and Broghamer on gear teeth, is expressed as [23]:

$$\begin{cases} K_f &= k_1 + \left(\dfrac{2y_A}{\rho_f}\right)^{k_2}\left(\dfrac{2y_A}{x_D - x_A}\right)^{k_3} \\ k_1 &= 0.3054 - 0.00489\phi_p^\circ - 0.000069\left(\phi_p^\circ\right)^2 \\ k_2 &= 0.3620 - 0.01268\phi_p^\circ + 0.000104\left(\phi_p^\circ\right)^2 \\ k_3 &= 0.2934 + 0.00609\phi_p^\circ + 0.000087\left(\phi_p^\circ\right)^2 \end{cases} \tag{31}$$

The geometric and loading parameters required for Eq. (30) are tabulated in Table 4. Figure. 16 graphically illustrates these parameters on the tooth profile.

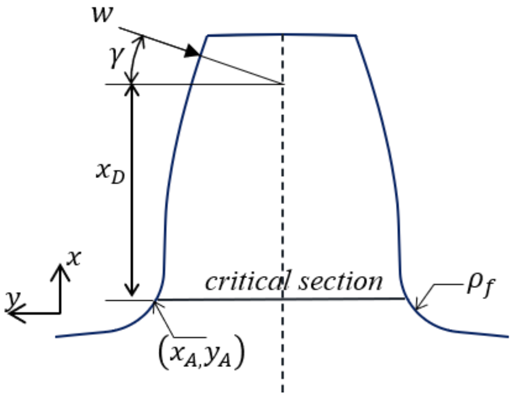

Figure 16. Tooth Profile with ISO-Fillet: $TAF\ \alpha = 1.0375\ z_1 = 40\ x_1 = -0.6305$

Table 4. ISO Fillet-stress parameters: $TAF\ \alpha = 1.0375\ z_1 = 40\ x_1 = -0.6305$

Parameter	Description	Source	Value
w	Load intensity	Section 5	300 N/mm
m	Module	Table 1	3 mm
γ	Load angle	CAD Model	18.407°
x_D	Moment arm location	CAD Model	59.422 mm
k_1, k_2, k_3	Stress-concentration constants	Eq. (31)	0.1800, 0.1500, 0.4500
(x_A, y_A)	Critical-section coordinates	CAD Model	54.9585, 2.5481
ρ_f	Fillet radius of curvature	Table 2	1.3 mm
K_f	Stress-concentration factor	Eq. (31)	1.483

Substitution into Eq. (30) gives $\sigma_t^A = 416.7$MPa, compared with 443 MPa from the present FEA for the same case, corresponding to a difference of 6.0%. The stress-concentration constants used above were calibrated by Dolan and Broghamer from photoelastic tests on gears with circular fillet geometry, consistent with the ISO fillet's own form. An equivalent check for the cutter-generated fillet would extrapolate this calibration beyond the circular-fillet geometry class on which it was established, and is therefore not reported as an independent validation. To the authors' knowledge, no published study reports experimental or independently-validated stress data for Altered Tooth-Sum Gears with cutter-generated root fillets under comparable geometry and loading conditions; the present cross-check therefore represents the closest available benchmark under the actual case-specific conditions of this study. Independent experimental validation specifically for the cutter-generated fillet in *ATG* configurations remains an important direction for future work.

8. CONCLUSIONS

The study extends cutter kinematics to the *ATG* framework to formulate root fillets directly from the relative motion between the rack cutter and the gear. Results for representative *ATG* configurations demonstrate that the deviation between the analytically generated fillets and ISO-based circular approximations increases markedly with the magnitude of negative profile shift, ranging from 6% to 12.47%, whereas ISO-based circular fillets generally provide adequate engineering representation for positive profile shifts, with deviations below 1.5 %. Consequently, FEM analysis of a representative *ATG* configuration with negative profile shift shows a 25% difference in root stress between the cutter-generated and ISO-based circular fillets, with maximum stresses of 332 MPa and 443 MPa, respectively. This difference is attributed to variations in fillet curvature distribution and critical-section thickness, which directly influence the computed root stress. The results therefore demonstrate the significant effect of root-profile deviation on predicted tooth-root stress and highlight the importance of representing the actual cutter-generated fillet for negatively shifted *ATG* configurations.

From an implementation perspective, the formulation is algebraic and requires only elementary trigonometric evaluation, allowing direct integration into CAD and finite element workflows. The present model assumes rigid-body kinematics under ideal rolling conditions and is restricted to spur gears generated by symmetric rack cutters. While the ISO-based fillet stress prediction was independently corroborated against a classical analytical method (Section 7), equivalent independent validation was not available for the analytically generated fillet because existing stress-concentration data are primarily calibrated for circular fillet geometries. Experimental validation to quantify deviations arising from manufacturing effects, together with extension of the formulation to other gear types, remains a topic for future investigation.

The proposed formulation is applicable to any involute spur gear, with its use particularly warranted for *ATG* configurations involving substantial negative profile shift, where the ISO approximation is shown to be least reliable. Overall, the proposed analytical approach establishes a consistent link between cutter kinematics and root fillet geometry, providing a basis for improved tooth-rootstress evaluation and the analysis and design of both standard and non-standard gearing systems, including *ATG* configurations.

NOMENCLATURE

$\boldsymbol{\alpha}$	Tooth-sum alteration factor	B	Backlash
$\boldsymbol{\beta}$	Center distance alteration factor	r	Radius of the rack tip
$\boldsymbol{\kappa}$	Profile shift factor	r_p	Radius of the pitch circle
$\boldsymbol{X_s}$	Total profile shift coefficient	r_w	Radius of the working circle
$\boldsymbol{x}$	Profile shift coefficient	r_b	Radius of the base circle
$\boldsymbol{\phi_p}$	Pressure angle at pitch circle	r_f	Radius of the fillet circle
$\boldsymbol{\phi_x}$	Pressure angle at location *x*	Y	Tooth topping coefficient
$\boldsymbol{\theta}$	Roll angle	z	Number of teeth
$\boldsymbol{p_c}$	Circular Pitch	z_s^a	Altered Tooth-sum
$\boldsymbol{m}$	Module	z_s^r	Reference tooth-sum
$\boldsymbol{c_s^r}$	Center distance of reference pair	ρ_f	Radius of the ISO circular fillet
$\boldsymbol{c_w^a}$	Working Center distance of *ATG*	ρ_l	Radius curvature-limit circle
$\boldsymbol{c_w}$	Working center distance	ρ_a	Radius curvature-addendum circle
$\boldsymbol{a}$	Addendum of rack		

ABBREVIATIONS

ATG	Altered tooth-sum gears	STG	Standard tooth-sum gears
TPSC	Total profile shift coefficient	TTC	Tooth topping Coefficient
TAF	Tooth-sum Alteration Factor	CAF	Center distance alteration Factor
PSF	Profile shift coefficient		

CONFLICTS OF INTEREST

The authors declare that there is no conflict of interest regarding the publication of this paper.

REFERENCES

[1] "ISO 6336-3: Calculation of load capacity of spur and helical gears — Part 3: Calculation of tooth bending strength," Geneva, 2019.

[2] A. A. Dsa and H. Lobo, "Analytical and geometric perspectives on altered tooth-sum spur gears within a unified non-dimensional gear design framework," *Mech. Mach. Theory*, vol. 225, p. 106455, Sep. 2026. doi: 10.1016/j.mechmachtheory.2026.106455.

[3] V. Mouton, E. Rigaud, C. Chevrel-Fraux, P. Casanova, and J. Perret-Liaudet, "Spur gear tooth root stress analysis by a 3D flexible multibody approach and a full-FE contact-based formulation," *Finite Elem. Anal. Des.*, vol. 242, p. 104264, Dec. 2024. doi: 10.1016/j.finel.2024.104264.

[4] J. I. Pedrero, M. B. Sánchez, M. Pleguezuelos, and A. Fuentes-Aznar, "Analysis of the tooth-root stress of external spur gears with high effective contact ratio," *Mech. Mach. Theory*, vol. 203, p. 105813, Nov. 2024. doi: 10.1016/j.mechmachtheory.2024.105813

[5] L. Bonaiti and C. Gorla, "Gear tooth root bending strength estimation under the assumption of fatigue limit existence," *Mater. Des. Process. Commun.*, vol. 2022, pp. 1–13, Jun. 2022. doi: 10.1155/2022/5056057.

[6] A. R. Rajesh, J. Gonsalvis, and K. A. Venugopal, "Load sharing analysis of bending strength in altered tooth-sum gears operating between a standard center distance and module," *Eur. J. Eng. Technol.*, vol. 3, no. 1, pp. 50–61, 2015.

[7] A. R. Rajesh, J. Gonsalvis, and K. A. Venugopal, "Investigation of tooth load distribution along the path of contact in altered tooth-sum gears," *J. Mod. Eng. Res.*, vol. 5, no. 4, pp. 42–50, 2015.

[8] A. R. Rajesh, J. Gonsalvis, and K. A. Venugopal, "Design and testing of gears operating between a specified center distance using altered tooth-sum gearing," *J. Mech. Eng. Autom.*, vol. 6, no. 5A, pp. 102–108, 2016.

[9] S. Krishnamurthy and R. Kurkal, "Bending stresses in profile corrected gears," in *Proc. Int. Conf. Recent Adv. Sci. Eng. (ICRASE)*, Dubai, UAE, Oct. 2023, p. 109. doi: 10.3390/engproc2023059109.

[10] T. J. Lisle, B. A. Shaw, and R. C. Frazer, "External spur gear root bending stress: A comparison of ISO 6336:2006, AGMA 2101-D04, ANSYS finite element analysis and strain gauge techniques," *Mech. Mach. Theory*, vol. 111, pp. 1–9, May 2017. doi: 10.1016/j.mechmachtheory.2017.01.006.

[11] A. C. Ram Kumar, N. Mohammed Raffic, K. Ganesh Babu, and S. Selvakumar, "Static structural analysis of spur gear using ANSYS 15.0 and material selection by COPRAS, MOORA techniques," *Mater. Today Proc.*, vol. 47, pp. 25–36, 2021. doi: 10.1016/j.matpr.2021.03.485.

[12] E. Can and M. Bozca, "Optimisation of gear geometrical parameters using KISSsoft," *Int. Sci. J. Mach. Technol. Mater.*, vol. 13, no. 1, pp. 7–10, 2019.

[13] S. Li, "Finite element analyses for contact strength and bending strength of a pair of spur gears with machining errors, assembly errors and tooth modifications," *Mech. Mach. Theory*, vol. 42, no. 1, pp. 88–114, Jan. 2007. doi: 10.1016/j.mechmachtheory.2006.01.009.

[14] R. Prabhu Sekar, "Performance enhancement of spur gear formed through asymmetric tooth," *Proc. Inst. Mech. Eng., Part J, J. Eng. Tribol.*, vol. 233, no. 9, pp. 1361–1378, Sep. 2019. doi: 10.1177/1350650119837822.

[15] R. Prabhu Sekar and G. Muthuveerappan, "Estimation of tooth form factor for normal contact ratio asymmetric spur gear tooth," *Mech. Mach. Theory*, vol. 90, pp. 187–218, Aug. 2015. doi: 10.1016/j.mechmachtheory.2015.03.019.

[16] F. L. Litvin, *Gear Geometry and Applied Theory*. Englewood Cliffs, NJ: Prentice Hall, 1994.

[17] M. C. Fetvaci and B. G. Şentürk, "Investigation of rack cutter geometry and trochoid curves at transverse section in gear manufacturing simulation," *J. Adv. Mech. Des. Syst. Manuf.*, vol. 18, no. 8, p. JAMDSM0098, 2024. doi: 10.1299/jamdsm.2024jamdsm0098.

[18] C. Spitas and V. Spitas, "A FEM study of the bending strength of circular fillet gear teeth compared to trochoidal fillets produced with enlarged cutter tip radius," *Mech. Based Des. Struct. Mach.*, vol. 35, no. 1, pp. 59–73, Feb. 2007. doi: 10.1080/15397730601182802.

[19] P. Dong, S. Zuo, S. Du, P. Tenberge, S. Wang, X. Xu, and X. Wang, "Optimum design of the tooth root profile for improving bending capacity," *Mech. Mach. Theory*, vol. 151, p. 103910, Sep. 2020. doi: 10.1016/j.mechmachtheory.2020.103910.

[20] A. Artoni, "Is the root fillet curve in involute gears trochoidal? A geometric reassessment," *Mech. Mach. Theory*, vol. 217, p. 106228, Dec. 2025. doi: 10.1016/j.mechmachtheory.2025.106228

[21] A. Dsa and J. Gonsalvis, "Enhancing design features of asymmetric spur gears operating on a specified center distance using tooth sum altered gear geometry," *Proc. Eng. Technol. Innov.*, vol. 18, pp. 1–14, Mar. 2021. doi: 10.46604/peti.2021.7074.

[22] G. Maitra, *Handbook of Gear Design*. New Delhi: Tata McGraw-Hill, 1994.

[23] J. R. Colbourne, *The Geometry of Involute Gears*. New York, NY: Springer New York, 1987.

[24] A. Dsa and J. Gonsalvis, "Tribological aspects affecting surface durability of tooth-sum altered spur gears: A load sharing approach," *Adv. Technol. Innov.*, vol. 8, no. 2, pp. 81–99, Apr. 2023. doi: 10.46604/aiti.2023.9562.

[25] "ISO 21771:2007, "Gears — Cylindrical involute gears and gear pairs — Concepts and geometry," Geneva, 2007.